Spectrochimica Acta Part B 65 (2010) 950–958

Contents lists available at ScienceDirect

Spectrochimica Acta Part B

journal homepage: www.elsevier.com/locate/sab

Improving the oxidation resistance of AlCrN coatings by tailoring chromium out-diffusion

R. Escobar Galindo [a,*], J.L. Endrino [a], R. Martínez [b], J.M. Albella [a]

[a] Instituto de Ciencia de Materiales de Madrid, Consejo Superior de Investigaciones Científicas, E-28049 Madrid, Spain
[b] AIN-Centro de Ingeniería Avanzada de Superficies, Cordovilla, E-31191 Pamplona, Spain

ARTICLE INFO

Article history:
Received 10 June 2010
Accepted 4 September 2010
Available online 16 September 2010

Keywords:
GDOES
AlCrN
Oxidation
Diffusion barrier

ABSTRACT

In this work, we have studied the improvement on the oxidation resistance of AlCrN-based coatings by adding a subsurface titanium nitride barrier layer. Since oxidation is interrelated with the inward diffusion of oxygen into the surface of $Al_xCr_{1-x}N$ ($x = 0.70$) coatings and the outward diffusion of Cr to the surface, the oxidation behaviour of the aluminium-rich AlCrN coatings can be tuned by designing the coating in an appropriate layered structure. The buried depth of the embedded layer and the oxidation time were varied, and the changes in the AlCrN/TiN depth composition profiles and surface oxidation stoichiometry were analysed by means of Glow Discharge Optical Emission Spectroscopy (GDOES) and Cross Sectional SEM (X-SEM) maps. It was observed that when a TiN diffusion barrier of 300 nm was deposited near the top surface (500 nm from the surface) the inhibition of the inward diffusion of oxygen and formation of beneficial alumina surface layers was promoted and consequently an increase of the oxidation resistance is achieved. This is explained in terms of a limited surplus of chromium from the coating to the surface. This was corroborated after performing experiments using CrN as embedded barrier layer which resulted in a continuous surplus of chromium to the surface and the formation of Cr-rich oxides. GDOES, in combination with X-SEM elemental maps, was proved to be a fast and accurate technique to monitor composition in-depth changes during oxidation, providing unique information regarding the oxide structure formation.

1. Introduction

Recently, Al–Cr–N based coatings have received increasingly attention of researchers and coating designers due to their excellent mechanical properties and superior oxidation resistance compared with Al–Ti–N based coatings [1–6]. It has been predicted by the band parameters method that the critical content of Al in Al–Cr–N from B1 (NaCl-type) to B4 (wurtzitic) is 77.2% in comparison to only 65.3% solubility in Al–Ti–N [7]. This higher aluminium content in a B1 cubic phase allows for increased formation of alumina-like tribofilms without sacrificing mechanical properties such as hardness. Alumina based tribofilms have been shown to protect forming and machining tools by redirecting more heat towards the workpiece [8,9]. Nevertheless, increasing aluminium content in the protective coating does not always guarantee the formation of alumina tribofilms since the enthalpy of formation of Cr_2O_3 is lower than that of Al_2O_3.

The oxidation mechanism of AlCrN thin films have been extensively studied in the literature. In the early 90's Hofmann [10] described this process in terms of metal inter-diffusion, originating a typical oxide multilayer structure. This multilayer is explained due to the different diffusivity of the metal species. Although Al_2O_3 is the more stable compound, chromium is the more mobile species and preferentially forms a surface oxide. This chromium oxide inhibits the diffusivity of aluminium, leading to a build-up of aluminium oxide beneath this layer. In turn, the aluminium-rich layer reduces the further out-diffusion of chromium and leads to a slightly increased chromium concentration underneath. Therefore, a structure with a mixed, Cr-rich, Cr/Al oxide layer at the film surface and an Al-rich, Cr/Al oxynitride in the bulk is formed. Lately, Banakh et al. [3] corroborated this model, suggesting the de-nitridation of the film and the formation of a Cr/Al mixed oxide as the oxidation mechanism. More recently, Lin et al. studied the oxidation process of AlCrN films by using differential scanning calorimetry (DSC) and thermogravimetric analysis (TGA) [11]. They concluded that, for the oxidation temperature ranging from 700 to 1050 °C, thermal energy is sufficient to facilitate outward diffusion of nitrogen atoms/ions towards the film surface (de-nitridation). At the same time they proposed that the diffusion of Cr and Al ions outwards and atomic oxygen inwards will promote the formation of a $(Cr, Al)_2O_3$ layer on the film surface, acting as a effective diffusion barrier slowing down the inward diffusion of oxygen.

Therefore, it is well documented that AlCrN coatings show high short-term oxidation resistance up to 1100 °C due to the formation of Cr–Al oxides that are lubricious and have strong diffusion barrier properties against further inward diffusion of oxygen into the films. In

* Corresponding author. Tel.: +34 91 3721420x330.
E-mail address: rescobar@icmm.csic.es (R. Escobar Galindo).

0584-8547/$ – see front matter © 2010 Elsevier B.V. All rights reserved.
doi:10.1016/j.sab.2010.09.005

particular Al-rich $Al_{70}Cr_{30}N$ coatings present excellent oxidation resistance due to the formation of alumina at the surface. However, more demanding applications such as gas turbine engines, die casting and moulding industries also require of long-term oxidation resistant coatings that can withstand exposure to oxygen and water vapour containing environments for their entire service lives. Under longer exposure times in air AlCrN coatings suffer a partial depletion of aluminium at the surface and a high diffusion of chromium is promoted. In this case, the formation of surface alumina is inhibited and chromium-rich complex $(Al, Cr)_2O_3$ oxide films are formed due to the solubility of Cr_2O_3 in alumina matrix [12].

In this work we have studied the incorporation of a subsurface TiN layer in the AlCrN coatings. This layer has been shown to act as a diffusion barrier in microelectronics [13–15] and can act as an excellent diffusion barrier of chromium ions. Here, we demonstrate that the TiN barrier promotes the formation of aluminium-rich oxides at the surface of the coating, improving the long-time oxidation resistance of the films. To achieve this goal, we have used Glow Discharge Optical Emission Spectroscopy (GDOES) as a depth profiling technique [16] due to its excellent potential to accurately monitoring composition surface and in-depth changes during oxidation. GDOES has been previously applied with success to study the internal oxidation of carburized steels [17], oxide scale formation in Fe–Cr alloys [18], and oxidation resistance of AlN/CrN superlattices [19] and complex TiAlCrSiYN coatings [20]. In addition, we have compared GDOES results on selected samples with Cross Sectional Scanning emission micrographs (X-SEM).

2. Experimental

2.1. Coating deposition

A front-loading Balzers' rapid coating system (RCS) machine has been employed for the deposition of the coatings in this study. The RCS machine is equipped with 6 cathode arc sources positioned at two different heights. Two of the six sources contained Ti targets and were used to deposit a 0.3 μm thick titanium nitride adhesion layer as well as to deposit a TiN subsurface diffusion barrier. The remaining four sources contained AlCr (70:30) targets which were employed to deposit the main AlCrN layer with a thickness of 3 μm in all the samples. In this study, 20 mm-diameter cold work tool steel coupons were used as substrates. During the deposition, the chamber was back-filled with pure reactive nitrogen to a pressure of 3.5 Pa and the temperature of the substrates was held at approximately 450 °C. Also, a substrate bias voltage of −100 V was applied to the substrates.

2.2. Multilayer characterisation

GDOES depth profile analysis of the coatings was completed using a Horiba Jobin Yvon RF GD Profiler equipped with a 4 mm diameter copper anode and operating in argon gas [21–23]. In previous works [24,25] Escobar Galindo et al. performed a complete optimization of the operating conditions for the analysis using this GDOES system. By applying a radio frequency discharge pressure of 650 Pa and a forward power of 40 W multilayers in the nanometre range were able to be analyzed. Therefore in this study we have kept fixed these operation settings. The emission responses from the excited sputtered elements were detected with a polychromator of focal length of 500 mm. The optical path of the spectrometer is nitrogen purged. The emission lines used were 130.21 nm for oxygen, 149.262 nm for nitrogen, 156.14 nm for carbon, 371.99 nm for iron, 396.15 nm for aluminium and 425.43 nm for chromium. The chamber was cleaned by sputtering a silicon (100) sample for 20 min prior to the measurements. This procedure minimises the surface contamination of the samples and allows a faster stabilisation of the plasma [26]. No memory effects were observed after this pre-sputtering procedure. Before every experiment, the samples were flushed with argon during 60 s. This is a typical procedure to remove the contaminants (carbon, oxygen, hydrogen) from the inner walls of the anode prior to the analysis of the sample and has been extensively applied by GDOES users. Molchan et al. have recently proposed [27] that this procedure can be improved by using a low-energy plasma (<5 W) to gently remove contaminant from the surface of the sample. The high etching rates obtained during GDOES analysis resulted in very short experimental times (below 1 min of operation). A collection rate of 200 points/second was used to measure all the samples. Quantified profiles were obtained automatically using the standard Jobin Yvon QUANTUM Intelligent Quantification (IQ) software. The setup was calibrated

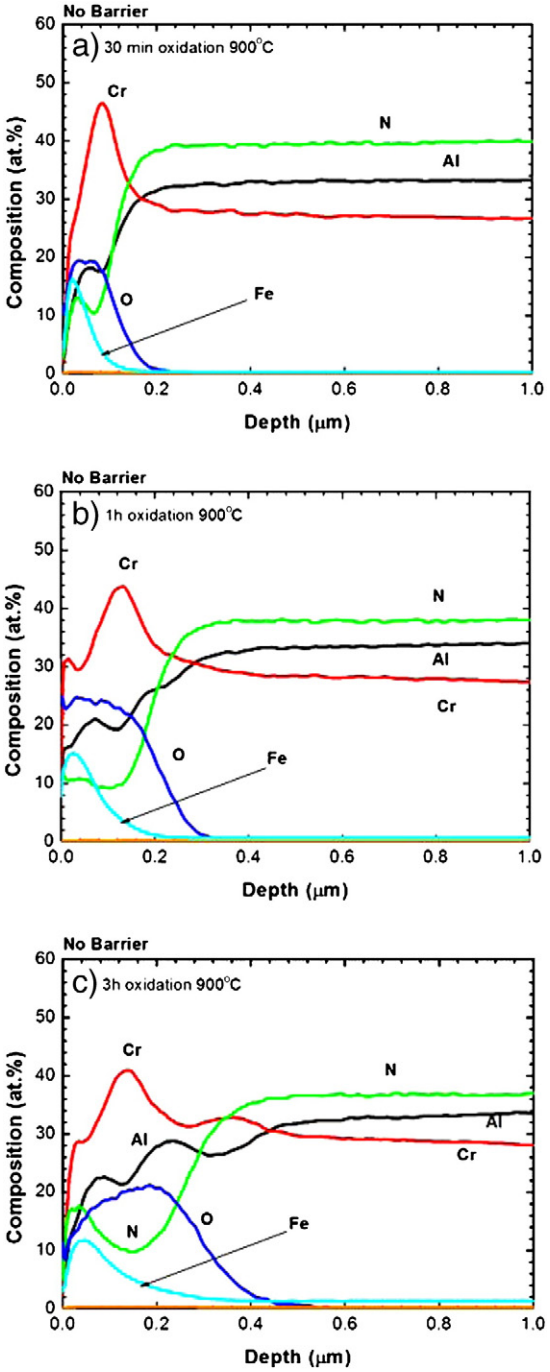

Fig. 1. GDOES profiles of AlCrN coatings without TiN barrier after oxidation in air at 900 °C for a) 30 min, b) 1 h and c) 3 h.

using standard materials of known composition. In order to improve the quantification of nitrogen, we have used a series of chromium nitride coatings deposited by magnetron sputtering in our laboratory [28]. The composition of these homemade standards was assessed by Rutherford Backscattering Spectroscopy (RBS). A Veeco Dektak 150 stylus surface profiler was used to measure the crater depths.

Isothermal oxidation tests were performed in air, at 900 °C during 0.5, 1, 3 and 24 h with each specimen placed in an alumina crucible.

Qualitative cross-sectional energy-dispersive X-ray spectroscopy (EDX) element mapping and images were obtained using an INCAx-sight Field Emission Scanning Electron Microscope (FE-SEM) with a resolution of 136 eV when operating at 5.9 keV.

3. Results and discussion

In Section 3.1, we describe the short and long-term oxidation kinetics of a single layer AlCrN coatings. Later in Section 3.2, we compare those results to the case of a multilayer AlCrN/TiN/AlCrN system by varying the buried depth of the TiN diffusion barrier (Section 3.2.1) as well as the oxidation time (Section 3.2.2). Finally in Section 3.3 we discuss the effectiveness of TiN as a diffusion barrier by studying the oxidation performance of a AlCrN/CrN/AlCrN multilayer system.

3.1. Oxidation performance of AlCrN

Fig. 1 shows the GDOES profiles of AlCrN coating without TiN barrier after a) 30 min, b) 1 h and c) 3 h oxidation at 900 °C. The thicknesses of the oxide layer formed after each oxidation time are reported in Table 1. For short oxidation times (Fig. 1a), there is a clear pileup of chromium near the surface revealing the formation of Cr-rich oxide layer on top of the AlCrN original coating. Within this oxidised layer the average Al/Cr content ratio remains low (0.47) as detailed in Table 1. The presence of Fe on the surface of the coating is observed even at short oxidation times, indicating a migration of substrate elements towards the surface .After increasing the oxidation time there is a clear growth of the thickness of the oxide layer (Fig. 1b–c). It can be also observed the progressive formation of an AlO_x layer below the CrO_x (note for example the “double peak” in the Al profile within the oxide layer of Fig. 1c). This behaviour can be explained in terms of the higher mobility of chromium to form a Cr-rich oxide layer. The diffusivity of aluminium is reduced through this chromium oxide layer and an Al-rich oxide is grown underneath generating an oxide multilayer structure as described by Hofmann [10]. The total Al/Cr ratio slightly increases after 1 and 3 h oxidation to 0.54 and 0.68, respectively, but there is no evidence of the formation of a beneficial aluminium rich oxide on the surface. After oxidation for 24 h the oxide layer was too porous and rough to be measured by the GDOES technique. In any case, the thickness of this grown scale can be estimated to be of larger than 4 μm by profilometry measurements. In Fig. 2a, the oxygen profiles of the films without oxidation and after 30 min, 1 h and 3 h oxidation are shown for comparison. The increase of the oxide layer thickness upon oxidation can be clearly observed and compared with the sample containing a TiN diffusion barrier (see Fig. 2b) as discussed below in Section 3.2.2.

Table 1
Oxide Thickness and Al/Cr ratio within the oxide for AlCrN samples oxidized at 900 °C with no diffusion barrier and with TiN or CrN barriers buried at a depth of 0.6 μm. The data are shown for different oxidation times.

Oxidation Time (h)	Diffusion Barrier	Oxide Thickness (nm)	Al/Cr oxide
0.5	No Barrier	115 ± 10	0.47 ± 0.08
	TiN	50 ± 5	0.71 ± 0.05
1	No Barrier	190 ± 20	0.54 ± 0.10
	TiN	85 ± 10	0.77 ± 0.20
3	No Barrier	300 ± 20	0.68 ± 0.16
	TiN	150 ± 10	0.92 ± 0.10
	CrN	280 ± 20	0.66 ± 0.08
24	No barrier	>4000	–
	TiN	1100 ± 50	1.00 ± 0.20

3.2. Oxidation performance of AlCrN/TiN/AlCrN multilayers

As previously stated, the main aim of this work is to control the oxidation behaviour of AlCrN coatings by the deposition of an intermediate diffusion barrier of TiN. In Fig. 3, a GDOES profile and X-SEM image and EDX element mapping of an as deposited AlCrN/TiN/AlCrN multilayer are shown. In this case, the diffusion barrier is buried at a depth of 700 nm from the surface. In the following sections we study the influence on the multilayer oxidation resistance of a) the depth of the TiN embedded layer and b) the oxidation time.

3.2.1. Effect of buried depth

A set of seven AlCrN samples was deposited containing an intermediate TiN layer at different depths from the surface (see Table 2). The samples were annealed in air during 3 h at 900 °C. Fig. 4 shows representative GDOES profiles of the oxidised samples for TiN buried depths of a) 2.8 μm, b) 2.3 μm, c) 1.1 μm, d) 0.7 μm and e) 0.5 μm respectively. The first difference in comparison to samples

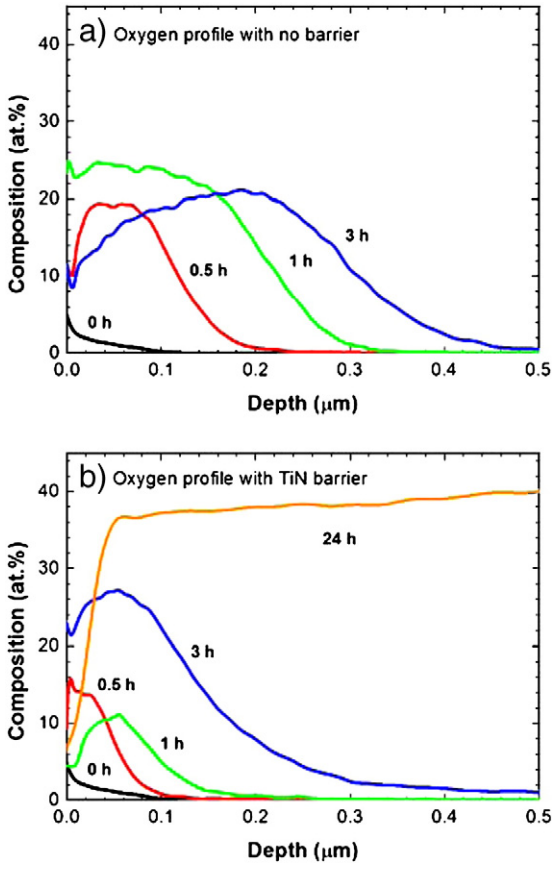

Fig. 2. (Left) GDOES oxygen profiles of AlCrN coatings without TiN barrier as deposited and after oxidation in air at 900 °C for 30 min, 1 h and 3 h. (Right) GDOES oxygen profiles of AlCrN/TiN coatings with TiN barrier buried at 0.6 μm as deposited and after oxidation in air at 900 °C for 30 min, 1 h, 3 and 24 h.

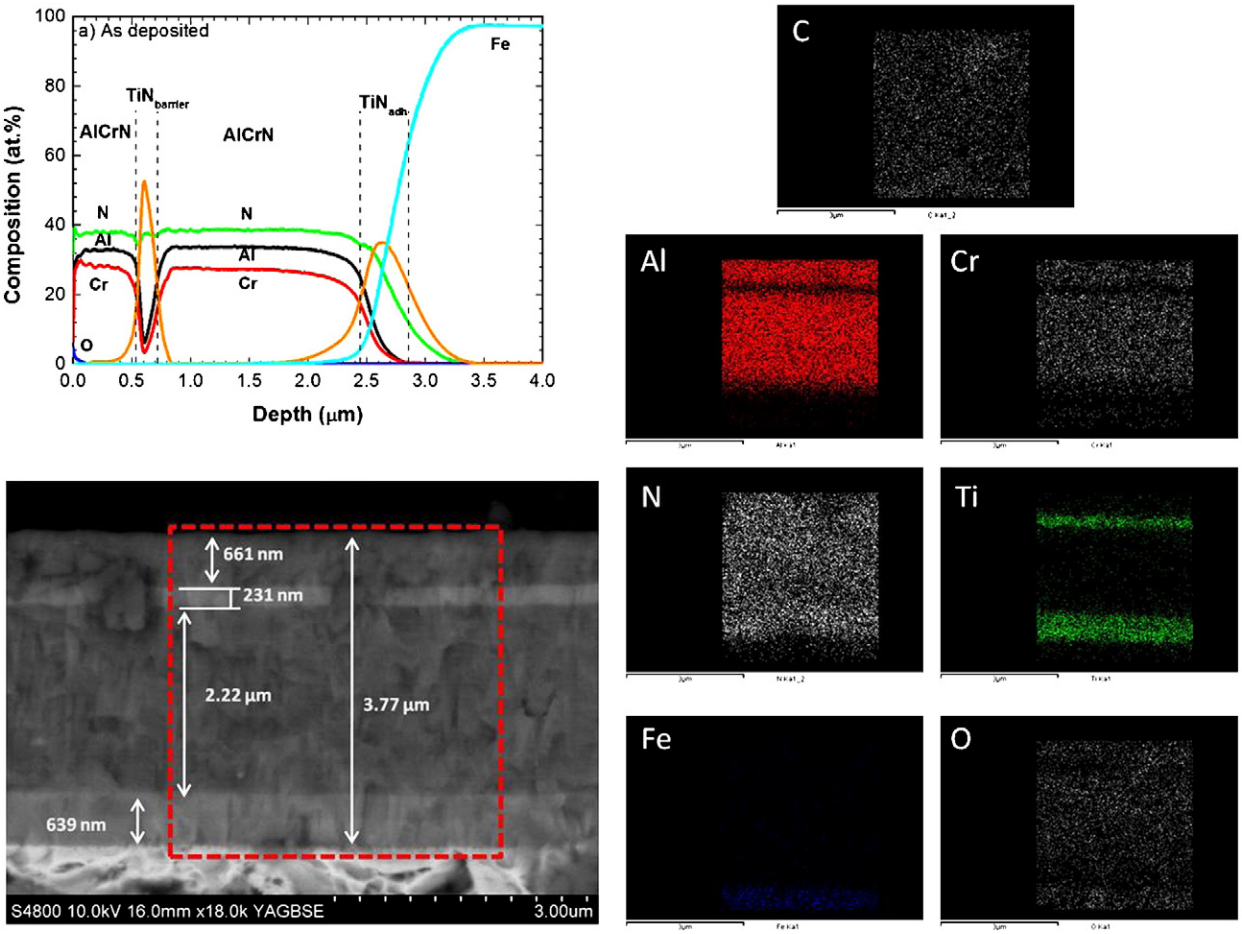

Fig. 3. GDOES profile (top-left) and cross sectional SEM image (bottom-left) of as deposited AlCrN/TiN coating with TiN barrier buried at 0.6 μm. The dotted square area delimitates the zone where elemental mapping was performed (see right panels for C, Al, Cr, N, Ti, Fe and O).

without TiN barrier (Fig. 1) is the thickness of the oxide layer formed. Clearly, the presence of the TiN barrier layer increases the overall oxidation resistance (approximately by a factor of 2) as can be observed in Table 2. After 3 h of oxidation the scale grown on the AlCrN coating without barrier is of more than 300 nm thick, while for the sample with the TiN is in the order of 150 nm for the same oxidation time, independently of the buried depth. Moreover there is a strong reduction of the Fe signal on the surface of the coatings. This indicates an inhibition of the migration of substrate elements towards the surface and underscores the benefits of incorporating a TiN barrier layer on the AlCrN coatings.

Table 2
Oxide Thickness and Al/Cr ratio within the oxide for AlCrN samples with TiN diffusion barrier oxidized at 900 °C for 3 h.

Buried depth (μm)	Oxide thickness (nm)	Al/Cr oxide
0.5	120 ± 10	1.05 ± 0.10
0.7	120 ± 10	0.78 ± 0.05
1.1	120 ± 10	0.58 ± 0.10
1.7	160 ± 15	0.57 ± 0.10
2.0	160 ± 15	0.61 ± 0.14
2.3	170 ± 20	0.51 ± 0.09
2.8	145 ± 15	0.40 ± 0.05

The main observation for samples with the TiN barrier layer deposited near the substrate (buried depth >1 μm Fig. 4a–c) is the formation of an extensive pile up of chromium as in the case of the coatings without TiN barrier (Fig. 1c). Previous XPS analysis revealed the formation of a Cr-rich oxide layer (mainly Cr_2O_3 [29,30]) on top of the AlCrN original coating. Within this oxidised layer the Al/Cr ratio for the sample with the barrier at 2.8 μm is similar to the sample with no barrier (0.4) as detailed in Table 2. However, as the barrier layer is being deposited closer to the surface it can be observed the progressive formation of an AlO_x layer below the Cr_2O_3 (note for example the "double peak" in the Al profile within the oxide layer of Fig. 4b and cc). Consequently, the Al/Cr ratio increases up to 0.5–0.6 for samples with the barrier buried at depths between 2.3 and 1.1 μm (see Table 2).

This mechanism dramatically changes when the TiN layer is deposited near the surface (buried depth <1 μm). In these samples, there is a clear evidence of aluminium enrichment at the surface as can be observed both in the GDOES profiles of Fig. 4c–d and in the EDX-SEM cross sectional mapping of Fig. 5. The formed oxide layers are thinner (100–120 nm) than for samples with the TiN closer to the substrate. The highest Al/Cr ratio in the oxidised layer (as high as 1.05) was obtained for the sample with the TiN layer buried at 0.5 μm (see Table 2). In particular, for this sample (see Fig. 4d), it is clear the formation of a 50 nm aluminium oxide film followed by a complex $AlCrO_x$ film. GDOES observations are supported by XPS measurements performed on this sample, where Al–O and Al–O–N bonds were predominant [6]. Hence, the presence of the TiN layer near the surface

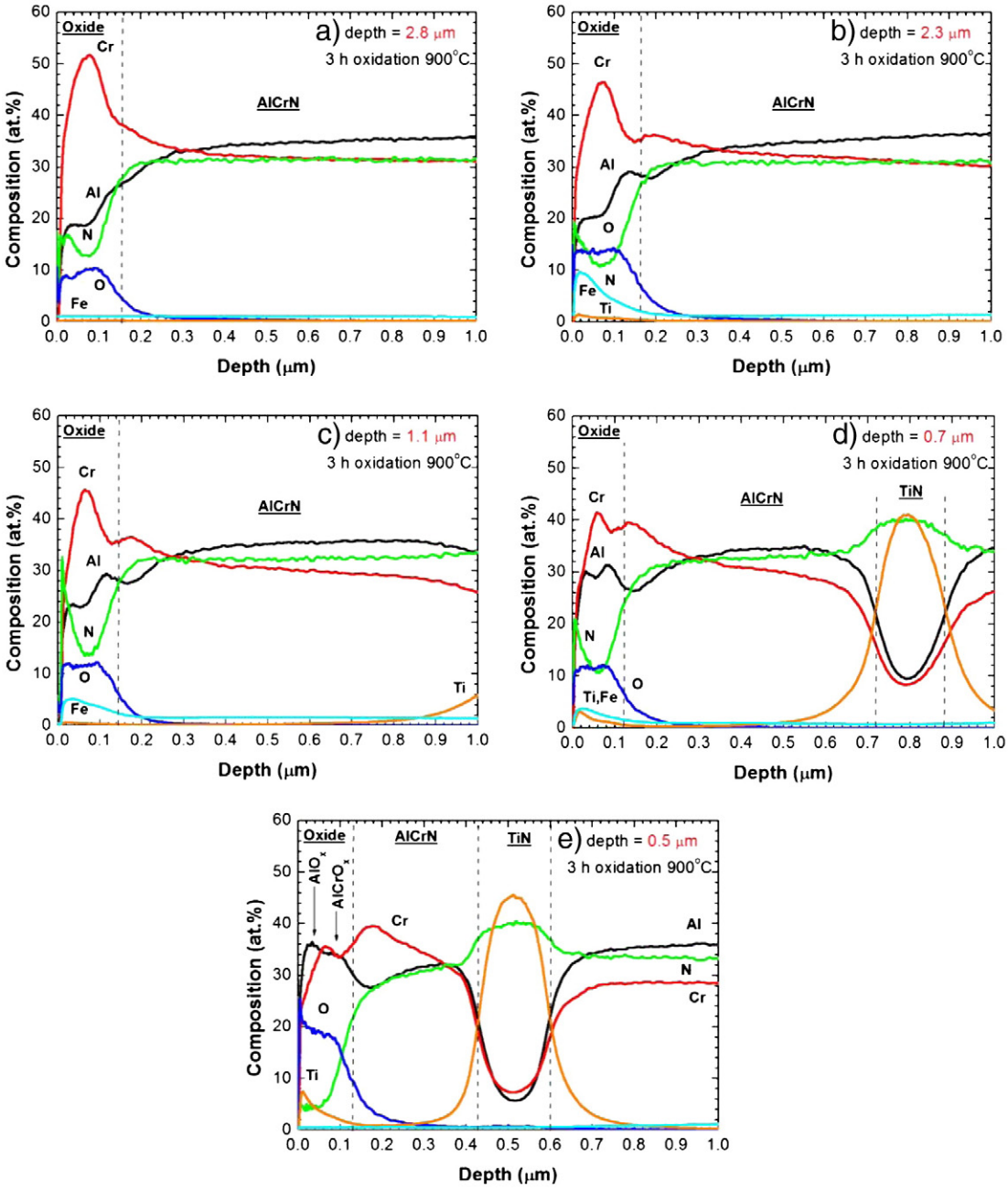

Fig. 4. GDOES profiles of AlCrN/TiN coatings after oxidation in air at 900 °C for 3 h with TiN barrier buried at a) 2.8 μm, b) 2.3 μm, c) 1.1 μm, d) 0.7 μm and e) 0.5 μm.

promotes the formation of a thinner and Al-rich oxide with a higher oxidation resistance due to the limited supply of Cr atoms to the surface.

3.2.2. Long-term oxidation

In the previous section, we have established the role that depositing a TiN buried layer near the surface has on the oxidation process of AlCrN coatings. In order to study the kinetics of such oxidation mechanism, TiN/AlCrN coatings were prepared by keeping both the oxidation temperature and the embedded depth constant at 900 °C and 0.6 μm, respectively, and varying the oxidation time. Here we perform a comparison of samples with and without a TiN barrier layer, prepared under the same conditions of oxidation time and temperature as discussed in Section 3.1. Table 1 summarised the samples studied.

Fig. 6a shows the detailed GDOES depth profiles for the as deposited AlCrN coating with a TiN barrier deposited at a fixed depth of 0.6 μm. The coating was then subjected to oxidation at 900 °C for b) 30 min, c) 1 h, d) 3 h and e) 24 h. After only 30 min oxidation, there is the formation of an oxide layer, with thickness of about 50 nm. This oxide layer consists of complex $AlCrO_x(N)$ compound (see Fig. 6b) and the Al/Cr ratio is markedly higher (0.71) than for the sample without diffusion barrier (0.47) for the same oxidation time (see Table 1). At this oxidation time, there was no evidence of Fe diffusion towards the surface. Increasing the oxidation time to one hour (see Fig. 6c) the oxide layer and the Al/Cr ratio grows up to 85 nm and 0.77, respectively. After 3 h of oxidation the nitrogen content of the oxide layer decreases, with a increasing migration of aluminium towards the surface. As discussed in the previous section, there is a clear separation of oxides with the formation of a sub-

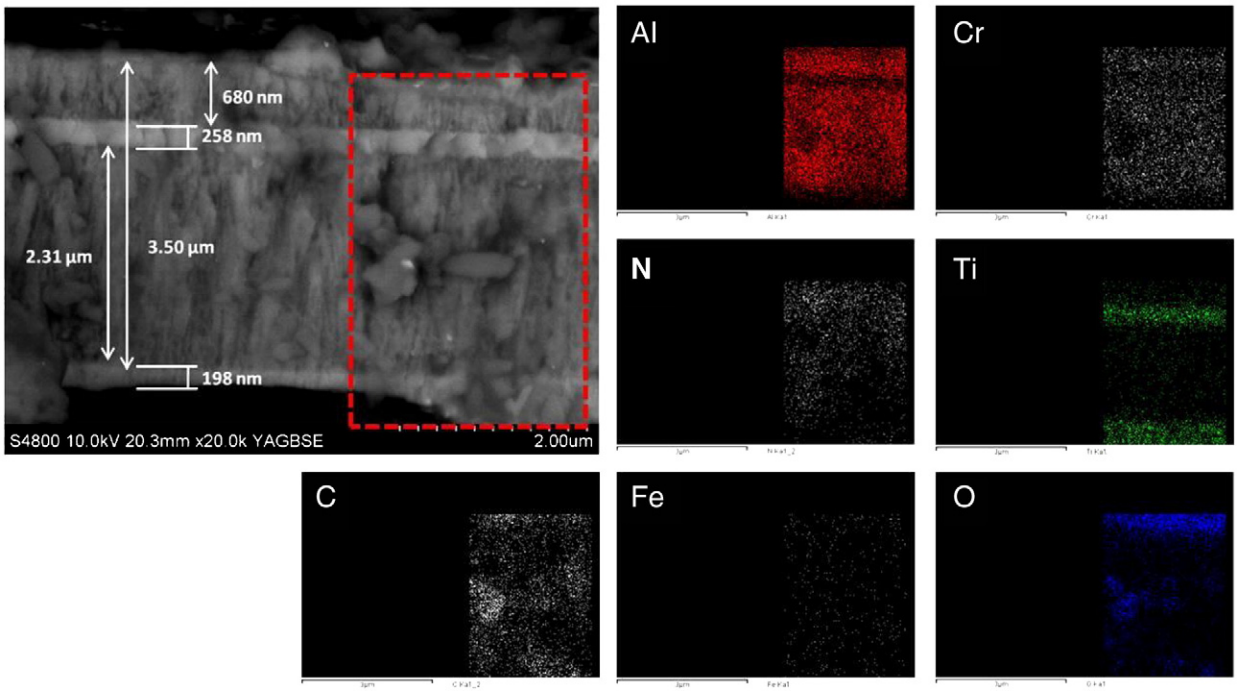

Fig. 5. Cross sectional SEM image (left) of as deposited AlCrN/TiN coating with TiN barrier buried at 0.7 µm. The dotted square area delimitates the zone where elemental mapping was performed (see right panels for C, Al, Cr, N, Ti, Fe and O).

stoichiometric AlO_x layer on top of the previously formed $AlCrO_x$ (see Fig. 6d). This is quantitatively evident as the Al/Cr ratio is much higher (0.92) than the value obtained for the sample without diffusion barrier (0.68). At this stage, there is some diffusion of titanium from the barrier layer to the surface and of iron from the substrate. Finally, after an oxidation time of 24 h (Fig. 6e), the oxide layer is thicker than 1 µm and the whole TiN buried layer disappears, migrating to the surface. The oxide layer consists of a stoichiometric alumina top layer (O/Al ratio is 1.5) and a subsurface $AlCrO_x$ as can be derived from the oscillations present in the Cr–Al profiles. The solution of Fe inside the layer is now more evident in accordance with observations made by Katesan for iron transport across alumina scales [31]. This multilayer structure is similar to the predicted by Hofmann model [10] although in our case the oxide top layer is alumina and not chromium oxide with the subsequent oxidation resistance improvement. Note also the practical disappearance of nitrogen at the surface of this sample, in accordance to the de-nitridation model proposed by Banakh et al. [3]. In Fig. 2b, the oxygen profiles of the films without oxidation and after 30 min, 1 h, 3 h and 24 h oxidation are shown for comparison with those obtained without TiN barrier layer (Fig. 2a).

3.3. Oxidation performance of AlCrN/CrN/AlCrN multilayers

In Section 3.1 we related the presence of the TiN buried layer, close to the surface, to the formation of Al-rich oxides due to the limited supply of Cr atoms to the surface. In order to corroborate this point, a CrN layer, which is a less effective diffusion barrier, was embedded into the AlCrN coating. By doing this, we assure that the supply of Cr atoms to the surface is not inhibited. The CrN barrier was deposited at a depth of 0.6 µm and the multilayer sample was oxidised at 900 °C for 3 h. Therefore the results can be compared to those obtained for AlCrN/TiN/AlCrN multilayer of Fig. 6d. Fig. 7 shows the GDOES depth profiles for a) the as deposited AlCrN/CrN/AlCrN sample and b) the sample after 3 h of oxidation. It is clear that the presence of CrN layer enhances the chromium content (Al/Cr ratio is 0.66) and the thickness (280 nm) of the oxide scale as compared with the sample containing the TiN barrier at similar depth and oxidation temperature (see Table 1). Moreover, the CrN layer completely diffuses to the surface and there is a segregation of iron carbide from the substrate at a depth of 900 nm, completely replacing the barrier layer. SEM EDX cross sectional mapping (shown in Fig. 8) corroborates the formation of a surface Cr-rich oxide and a subsurface FeC_x layer.

Finally, in Fig. 9 we present, for comparison purposes, the width of the grown oxide versus the oxidation time for samples oxidised at 900 °C with a) no barrier, b) TiN barrier and c) CrN barrier. The beneficial effect of the presence of the TiN diffusion barrier layer near the surface can be clearly observed. It significantly reduces the oxygen inward diffusion into the layer and consequently results in an increase in oxidation resistance at longer oxidation times. As can be seen in the inset of Fig. 9, for short oxidation times (up to 3 h) the grown of the oxide follows a parabolic law,

$$x = Bt^{1/2} \tag{1}$$

where x is the thickness of the growing oxide, B is the parabolic rate constant, and t is the oxidation time [32]. It is evident that the rate of oxide formation is higher for samples with no barrier ($B = 2.9 \pm 0.4$ nm $s^{-1/2}$) than when a TiN barrier is present ($B = 1.6 \pm 0.1$ nm $s^{-1/2}$). Moreover, although for samples with no barrier the oxide start growing from very short oxidation times, for samples with the TiN barrier there is an incubation time prior to the formation of the scale (see the interception of the fitted line with the x-axis).

4. Conclusions

In this work we have studied the oxidation resistance improvement of $Al_{70}Cr_{30}N$ coatings by tailoring a multilayer structure. To this

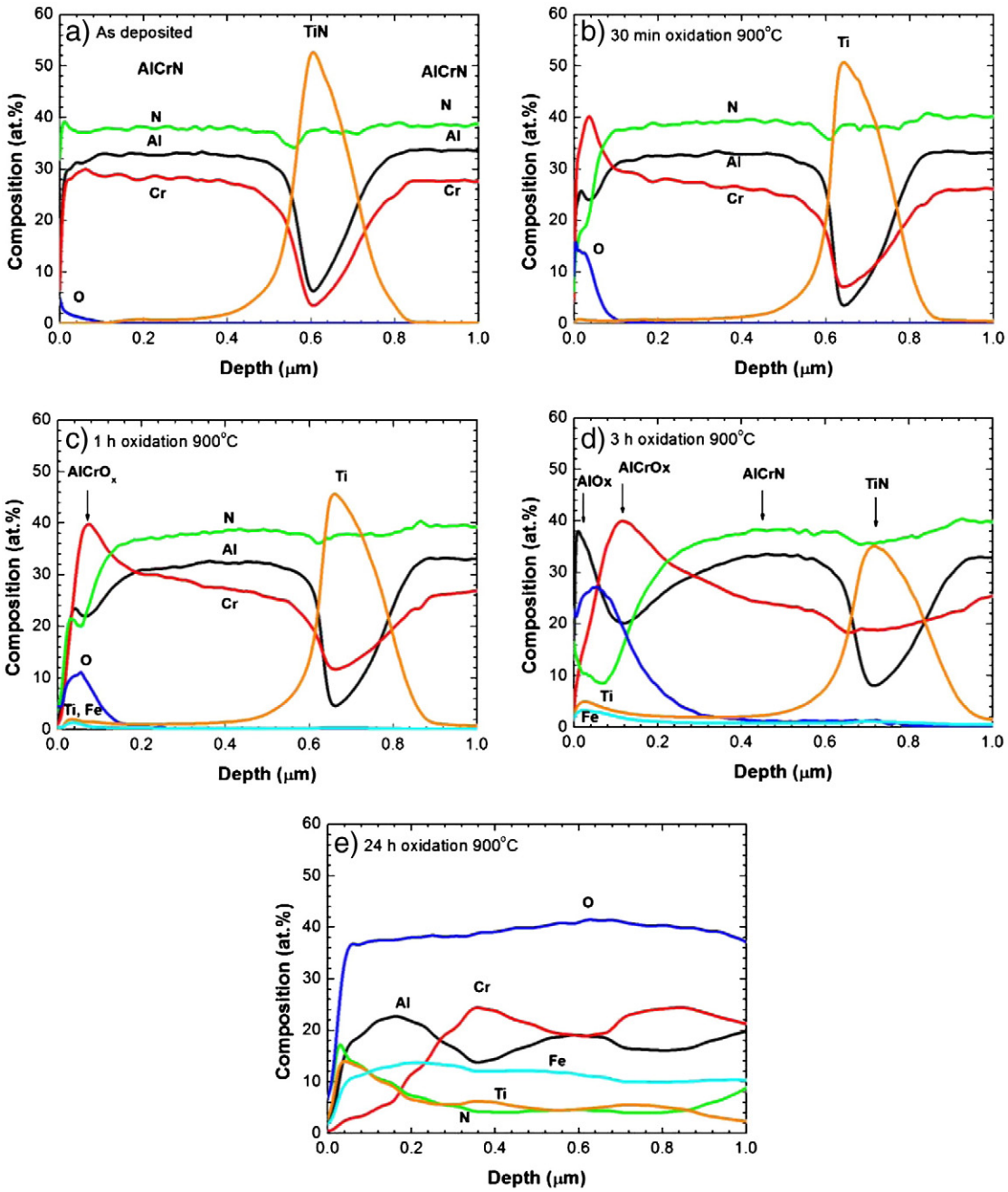

Fig. 6. GDOES profiles of AlCrN/TiN coatings with TiN barrier buried at 0.6 μm, a) as deposited and after oxidation in air at 900 °C for b) 30 min, c) 1 h, d) 3 h and e) 24 h.

purpose we have employed GDOES and cross sectional SEM as analytical techniques. GDOES is a superb tool for oxidation and diffusion studies thanks to its high erosion rate (>2 μm min^{-1}), sampling rate (>100 s^{-1}) and precision (in the nanometer range), allowing the analysis of a large number of samples under different preparation conditions (i.e. oxidation time and temperature). In combination with X-SEM elemental maps, GDOES provides unique information regarding the oxide structure formation due to its superb accuracy to monitor in-depth compositional changes during oxidation.

GDOES and X-SEM results indicated that, upon oxidation of an AlCrN single layer, Cr-rich oxides and oxynitrides are formed due to the high amount of Cr available for outward diffusion. However, the deposition of a diffusion barrier such as TiN embedded near the surface (<1 μm) improves the oxidation resistance of the AlCrN-based coatings by:

- decreasing the outward diffusion rate of Cr.
- promoting the formation of alumina rather than chromium oxide.
- significantly increasing the Al ratio within the surface oxidised layer.
- reducing the oxide inward diffusion (up to 24 h oxidation at 900 °C).
- inhibiting the migration of substrate elements to the surface.

Similar experiments carried out using CrN as embedded diffusion layers did not result in any oxidation resistance improvement. The deposition of such layers implies a continuous Cr surplus to the surface and therefore they do not prevent Cr out-diffusion as in the case of TiN layers.

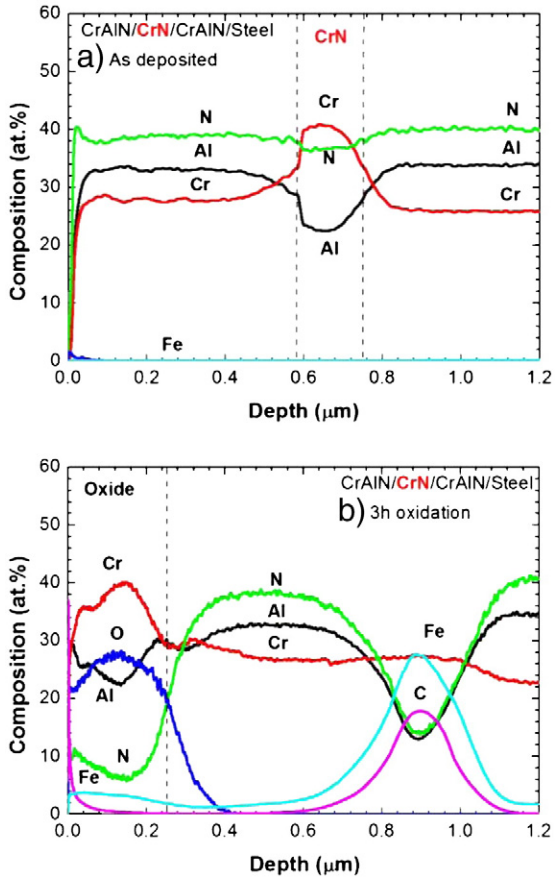

Fig. 7. GDOES profiles of AlCrN/CrN coatings with CrN barrier buried at 0.6 μm, a) as deposited and b) after oxidation in air at 900 °C for 3 h.

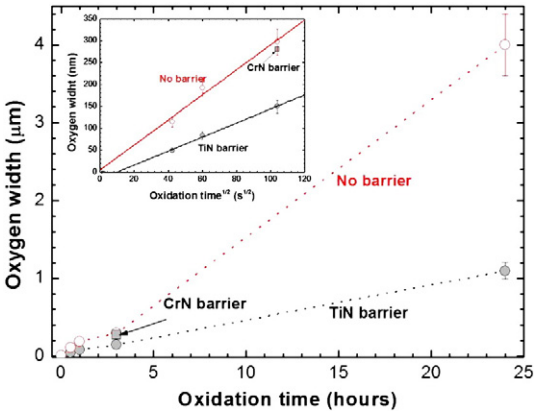

Fig. 9. Oxide thickness versus oxidation time for AlCrN without barrier (open circles), AlCrN/TiN multilayer (closed circles) and AlCrN/CrN multilayer (closed square) oxidized in air at 900 °C. In the inset the oxide thickness is plotted versus the square root of the oxidation time to show the parabolic oxide growth for short oxidation times (up to 3 h).

Acknowledgments

This work was financially supported by the Spanish Ministry of Science and Innovation (Project FUNCOAT, ref. CSD2008-00023). REG and JLE would like also to acknowledge the financial support from the Ramon y Cajal programme.

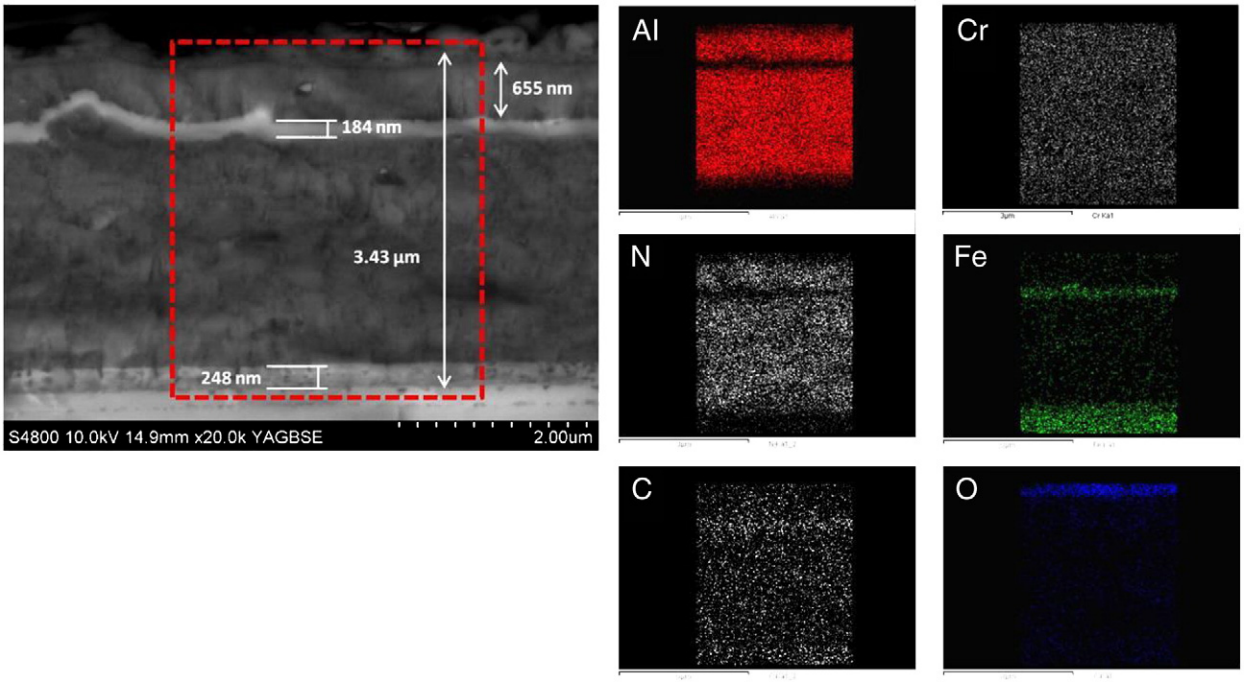

Fig. 8. Cross sectional SEM image (left) of AlCrN/CrN coating with CrN barrier buried at 0.6 μm after oxidation in air at 900 °C for hours. The dotted square area delimitates the zone where elemental mapping was performed (see right panels for Al, Cr, N, Fe, C and O).

References

[1] B. Mishra, C. Yamauchi (Eds.), TMS Annual Meeting, vol. 2, 2000, p. 291.
[2] M. Hirai, Y. Ueno, T. Suzuki, W. Jiang, C. Grigoriu, K. Yatsui, Characteristics of (Cr_{1-x}, Al_x) N films prepared by pulsed laser deposition, J. Appl. Phys. 40 (2001) 1056.
[3] O. Banakh, P.E. Schmid, R. Sanjinés, F. Lévy, High-temperature oxidation resistance of $Cr_{1-x}Al_xN$ thin films deposited by reactive magnetron sputtering, Surf. Coat. Technol. 163–164 (2003) 57–61.
[4] A.E. Reiter, V.H. Derflinger, B. Hanselmann, T. Bachmann, B. Sartory, Investigation of the properties of $Al_{1-x}Cr_xN$ coatings prepared by cathodic arc evaporation, Surf. Coat. Technol. 200 (2005) 2114–2122.
[5] K. Bobzin, E. Lugscheider, O. Knotek, M. Maes, Investigations of the Effect of PVD (Cr,Al)N Coatings Microstructure on Impact Toughness in Surface Engineering 2004 — Fundamentals and Applications, in: S.N. Basu, J.E. Krzanowski, J. Patscheider, Y. Gogotsi (Eds.), Mater. Res. Soc. Symp. Proc., 843, 2005, p. T1.2, Warrendale, PA.
[6] J.L. Endrino, A. Reiter, G.S. Fox-Rabinovich, J. Dosbaeva, R. Escobar Galindo, J.M. Albella, J.F. Marco, Oxidation tuning in AlCrN coating, Surf. Coat. Technol. 201 (2007) 4505–4511.
[7] Y. Makino, Application of band parameters to materials design, ISIJ Int. 38 (1998) 925–934.
[8] G.S. Fox-Rabinovich, K. Yamomoto, S.C. Veldhuis, A.I. Kovalev, G.K. Dosbaeva, Tribological adaptability of TiAlCrN PVD coatings under high performance machining conditions, Surf. Coat. Technol. 200 (2005) 1804–1813.
[9] J.L. Endrino, G.S. Fox-Rabinovich, R. Escobar Galindo, W. Kalss, S. Veldhuis, L. Soriano, J. Andersson, A. Gutiérrez, Oxidation post-treatment of hard AlTiN coating for machining of hardened steels, Surf. Coat. Technol. 204 (2009) 256–262.
[10] S. Hofmann, Formation and diffusion properties of oxide films on metals and on nitride coatings studied with Auger electron spectroscopy and X-ray photoelectron spectroscopy, Thin Solid Films 193–194 (1990) 648–664.
[11] J. Lin, B. Mishra, J.J. Moore, W.D. Sproul, A study of the oxidation behaviour of CrN and CrAlN thin films in air using DSC and TGA analyses, Surf. Coat. Technol. 202 (2008) 3272–3328.
[12] G.S. Fox-Rabinovich, G.C. Weatherley, A.I. Dodonov, A.I. Kovalev, L.S. Schuster, S.C. Veldhuis, G.K. Dosbaeva, Nano-crystalline filtered arc deposited (FAD) TiAlN PVD coatings for high-speed machining applications, Surf. Coat. Technol. 177–178 (2004) 800–811.
[13] S. Kanamori, T. Matzumoto, Suppression of platinum penetration failure in Ti/Pt/Au beam lead metal systems using a TiN diffusion barrier, Thin Solid Films 110 (1983) 205–213.
[14] S. Kanamori, Investigation of reactively sputtered TiN films for diffusion barriers, Thin Solid Films 136 (1986) 195–214.
[15] N. Kumar, M.G. Fissel, K. Pourrezaei, B. Lee, E.C. Douglas, Growth and properties of TiN and TiOxNy diffusion barriers in silicon on sapphire integrated circuits, Thin Solid Films 153 (1987) 287–301.
[16] J. Pisonero, B. Fernández, R. Pereiro, N. Bordel, A. Sanz-Medel, Glow-Discharge Spectrometry for Direct Analysis of Thin and Ultra-Thin Solid Films, Trends Anal. Chem. 25 (2006) 11–18.
[17] X. An, J. Cawley, W.M. Rainforth, L. Chen, A study of internal oxidation in carburized steels by glow discharge optical emission spectroscopy and scanning electron microscopy, Spectrochim. Acta Part B 58 (2003) 689–698.
[18] T. Horita, Y. Xiong, H. Kishimoto, K. Yamaji, N. Sakai, H. Yokokawa, Application of Fe–Cr alloys to solid oxide fuel cells for cost-reduction: oxidation behaviour of alloys in methane fuel, J. Power Sources 131 (2004) 293–298.
[19] B.S. Kim, G.S. Kim, S.Y. Lee, B.Y. Lee, Effects of Al target power on the mechanical and oxidation resistance of the CrN/AlN multilayer coatings, Surf. Coat. Technol. 202 (2008) 5526–5529.
[20] G.K. Dosbaeva, S.C. Veldhuis, K. Yamamoto, D.S. Wilkinson, B.D. Beake, N. Jenkins, A. Elfizy, G.S. Fox-Rabinovich, Oxide scales formation in nano-crystalline TiAlCrSiYN PVD coatings at elevated temperature, Int. J. Refract. Met. H. 28 (2010) 133–141.
[21] R. Payling, D. Jones, A. Bengtson, Glow discharge optical emission spectrometry, John Wiley and Sons, 1997.
[22] R. Winchester, R. Payling, Radio-frequency glow discharge spectrometry: A critical review, Spectrochim. Acta Part B 59 (2004) 607–666.
[23] http://www.jobinyvon.com/.
[24] R. Escobar Galindo, E. Forniés, J.M. Albella, Interfacial effects during the analysis of multilayer metal coatings by radio-frequency glow discharge optical emission spectroscopy: Part 1. Crater shape and sputtering rate effects, J. Anal. At. Spectrom. 20 (2005) 1108–1115.
[25] R. Escobar Galindo, E. Forniés, J.M. Albella, Interfacial effects during the analysis of multilayer metal coatings by radio-frequency glow discharge optical emission spectroscopy: Part 2. Evaluation of depth resolution function and application to thin multilayer coatings, J. Anal. At. Spectrom. 20 (2005) 1116–1120.
[26] R. Escobar Galindo, R. Gago, D. Duday, C. Palacio, Towards nanometric resolution in multilayer depth profiling: RBS, SIMS, XPS and GDOES comparative study, Anal. Bioanal. Chem. 396 (2010) 2725–2740.
[27] I.S. Molchan, G.E. Thompson, P. Skeldon, N. Trigoulet, P. Chapon, A. Tempez, J. Malherbe, L. Lobo Revilla, N. Bordel, Ph. Belenguer, T. Nelis, A. Zahri, L. Therese, Ph. Guillot, M. Ganciu, J. Michleri, M. Hohl, The concept of plasma cleaning in glow discharge spectrometry, J. Anal. At. Spectrom. 24 (2009) 734–741.
[28] R. Escobar Galindo, E. Forniés, R. Gago, J.M. Albella, Calibration of nitrogen content for GDOES depth profiling of complex nitride coatings, J. Anal. At. Spectrom. 22 (2007) 1512–1516.
[29] R. Sanjinés, O. Banakh, C. Rojas, P.E. Schmid, F. Lévy, Electronic properties of $Cr_{1-x}Al_xN$ thin films deposited by reactive magnetron sputtering, Thin Solid Films 420–421 (2002) 312–317.
[30] I. Milosev, H.-H. Strehblow, B. Navinsek, Comparison of TiN. ZrN and CrN hard nitride coatings: Electrochemical and thermal oxidation, Thin Solid Films 303 (1997) 246–254.
[31] K. Natesan, Corrosion performance of iron aluminides in mixed-oxidant environments, Mater. Sci. Eng. A 258 (1998) 126–134.
[32] G. Salomonsen, N. Norman, O. Lonsjo, T.G. Finstad, Kinetics and mechanism of oxide formation on Cr thin films, J. Phys. Condens. Matter 1 (1989) 7843–7850.